Photoinduced p- to n-type Switching in Thermoelectric Polymer-Carbon Nanotube Composites

ADVANCED MATERIALS
www.advmat.de

www.MaterialsViews.com

Photoinduced p- to n-type Switching in Thermoelectric Polymer-Carbon Nanotube Composites

Bernhard Dörling, Jason D. Ryan, John D. Craddock, Andrea Sorrentino, Ahmed El Basaty, Andrés Gomez, Miquel Garriga, Eva Pereiro, John E. Anthony, Matthew C. Weisenberger, Alejandro R. Goñi, Christian Müller, and Mariano Campoy-Quiles**

A broad range of organic electronic applications rely on the availability of both p- and n-type organic semiconductors, and the possibility to deposit them as sequential layers or to form spatial patterns. Examples include transport layers in diodes (OLEDs, photovoltaics, etc.), the transistor technology that underpins complementary logic and circuitry, as well as the p- and n-legs of a thermoelectric generator. Typically, a judicious selection of orthogonal solvents coupled with additive patterning techniques, such as inkjet-printing, is employed to provide patterned p- and n-regions in solution-processed devices. If higher resolution is required (below ≈100 µm), multistep lithographic methods are then compulsory. Here we show that combining a p-type semiconducting polymer with nitrogen doped n-type multiwalled carbon nanotubes (CNTs) results in composites whose majority carriers can be tuned by varying the relative composition. More importantly, we demonstrate UV photoinduced switching of an initially p-type composite solution into an n-type material, and present a proof of principle flexible thermoelectric generator with 15 double legs, which was fabricated from solution using a single processing step. Our results open the possibility of defining p- and n-type semiconductor patterns through UV treatment applied during solution deposition, with the potential to substantially simplify device production.

B. Dörling, Dr. A. El Basaty, A. Gomez, Dr. M. Garriga, Prof. A. R. Goñi, Dr. M. Campoy-Quiles
Institut de Ciència de Materials de Barcelona (ICMAB-CSIC)
Campus de la UAB
Bellaterra 08193, Spain
E-mail: mcampoy@icmab.es

J. D. Ryan, Dr. C. Müller
Department of Chemistry and Chemical Engineering
Chalmers University of Technology
Göteborg 41296, Sweden
E-mail: christian.muller@chalmers.se

J. D. Craddock, Prof. J. E. Anthony, Dr. M. C. Weisenberger
Center for Applied Energy Research
University of Kentucky
Lexington, KY 40511, USA

Dr. A. Sorrentino, Dr. E. Pereiro
ALBA Synchrotron Light Source
08193 Cerdanyola del Vallés, Spain

Dr. A. El Basaty
Department of Basic Science
Faculty of Industrial Education
Helwan University
Cairo, Egypt

Prof. A. R. Goñi
ICREA
Passeig Lluís Companys 23, 08010 Barcelona, Spain

DOI: 10.1002/adma.201505521

The performance of organic semiconductor based technologies is increasing rapidly in areas such as photovoltaic cells[1,2] and thermoelectric generators.[3–6] One key advantage of this class of materials is their amenability to solution processing, and thus potential for roll-to-roll upscaling.[7,8] The fully low-cost potential relies, however, on achieving realistic performance while keeping the processing schemes simple, including patterning of different materials.[9–11]

Organic thermoelectric generators offer the potential for a cost-effective technology to harvest low temperature waste heat.[8,11] While it is possible to build complete thermoelectric modules from a single type of thermoelectric material (either p- or n-type) and interconnect them with a regular conductor, only half of the legs will actually generate a thermovoltage. A more efficient device combines p- and complementary n-type materials by electrically connecting them in series and thermally in parallel in an alternating fashion. The fabrication of such modules will surely benefit from simple fabrication methods that allow patterning of regions of both types of material within one substrate.

To benchmark thermoelectric materials, the dimensionless figure of merit $ZT = S^2\sigma T/\kappa$ is typically used, where S is the Seebeck coefficient ($S > 0$ for p-type and $S < 0$ for n-type semiconductors), σ the electrical conductivity, κ the thermal conductivity, and T the average absolute temperature. In this context, polymers offer remarkably low κ values, in the range from 0.5 W m^{-1} K^{-1} down to 0.1 W m^{-1} K^{-1} (cf. Bi_2Te_3 exhibits $\kappa \approx 1.2$ W m^{-1} K^{-1}, while other typical inorganic semiconductors such as crystalline silicon have κ values ≈100 W m^{-1} K^{-1}).[12,13] Interestingly, the thermal conductivity of bulk polymers as well as conjugated macromolecules can be tuned by controlling molecular orientation.[14–16] In order to increase the modest electrical conductivity of polymers, a number of strategies have been proposed, including careful doping,[4,11,17–21] making composites of polymers with conductive fillers such as CNTs,[22–24] or fabricating multilayer composite

structures.[3] While these strategies have thus far worked relatively well for p-type materials, examples of air-stable, solution processable, n-type organic materials are scarce. For example, extrinsic doping of an n-type polymer in vacuum has proven to be inefficient due to large scale phase segregation.[6] A more direct, molecular design approach of the side chains of a small molecule has shown potential,[5] exhibiting good performance inside a glovebox. Another promising n-type material are CNTs, which are intrinsically ambipolar when protected from air, and have been shown to work as both p-type and n-type thermoelectric materials.[25–29] Their doping level, and concomitant Seebeck coefficient, can be tuned by doping electrically[30] or chemically with a variety of air-stable compounds.[31] Pure CNTs exhibit, however, a high thermal conductivity[32] and are difficult to process from solution. Using CNTs as conductive fillers within polymer matrices may result in synergies, such as a high S and σ, while keeping κ low and allowing for easy processing. In fact, it has been shown that van der Waals interactions can result in the polymer wrapping itself along or around the CNTs, which improves the processability of the CNTs.[33] The efficiency and selectivity to particular CNT chiralities depends on a variety of factors, such as the type of polymer (determining the specific π–π interactions), the molecular weight of the polymer, and the length and type of side chains.[34–37]

Here, we set out to investigate if n-type organic composites could be obtained by mixing a p-type conjugated polymer with nitrogen doped n-type CNTs. We chose poly(3-hexylthiophene) (P3HT) since it can show ambipolar transport[38] and can wrap around CNTs.[36] A moderate regioregularity of RR > 90% was selected in order to not limit the solubility of the polymer. Composites of regular, unmodified CNTs and doped P3HT have been shown to deliver power factors around 95 μW m^{-1} K^{-2}.[24] Here, composites with different stoichiometries were prepared by dispersing nitrogen doped CNTs (hereafter referred to simply as CNT) in *o*-dichlorobenzene (oDCB) and dissolving P3HT in chloroform, followed by mixing, sonicating, and drop-casting on flexible PET substrates (see the Experimental Section for details). Scanning electron microscopy (SEM) images of composites of P3HT and nitrogen doped multiwalled CNTs with low CNT content, c, appear well dispersed, while samples containing large fractions of CNTs exhibit agglomeration (**Figure 1**a). In all cases we observe fibrillar structures, which are likely CNT bundles wrapped with polymer. Moreover, atomic force microscopy (AFM) images reveal an increase in surface roughness of the films with increasing CNT content (Figure 1b). The low CNT content films clearly show a fine fibrillar structure with an average bundle diameter of 55 ± 15 nm, which is significantly smaller than for the high CNT content samples with 90 ± 30 nm (Figure 1a,b). We employed transmission X-ray microscopy (TXM) to confirm that the CNTs are distributed homogeneously all throughout the thickness of the film, as well as on the surface (Figure 1c). TXM also reveals the presence of iron-rich clusters in the sample, that is, residual catalyst from the CNT synthesis.[39,40] After acid cleaning of the CNT batch, the content of iron was reduced from 37 to 20 wt%, as estimated by elemental analysis and this reduction was confirmed by energy-dispersive X-ray spectroscopy. While an accurate quantitative analysis is complicated, these values can serve as an upper bound for iron content. Electrically, the composites consist of highly conductive, CNT-rich regions surrounded by polymer-rich regions that exhibit circa four orders of magnitude lower electrical conductivity (Figure 1d and Figure S1, Supporting Information). The percentage of highly electrically conducting areas increases with increasing CNT content as expected, while the acid treatment results in similar percentages but smaller domains. Histograms of current maps (Figure S1, Supporting Information) suggest that the purity of the domains is higher for acid-treated samples. Macroscopically, drop cast films on PET substrates present an electrically percolating behavior as a function of CNT content, with a percolation threshold around $c_p \approx 3.5$ wt% (**Figure 2**a), similar to earlier results.[24] This threshold points to relatively well dispersed carbon nanotubes, in agreement with the SEM, AFM, and TXM data shown in Figure 1. The macroscopic σ also increases sharply, in this case by five orders of magnitude, when comparing the neat polymer and composites with CNT weight fractions above percolation. Interestingly, the Seebeck coefficient varies from that of the neat polymer (≈1000 μV K^{-1})[24] to that of the CNTs (≈−10 μV K^{-1}) and correlates well with the percolation threshold observed for σ (Figure 2b). Strikingly, at around $c_s \approx 40$ wt% CNT content, the Seebeck coefficient changes sign. The corresponding power factor has two regimes, accordingly, separated by a zero value. Simple modules can be fabricated using these composites, with p-legs with $c = 20$ wt%, and n-legs with $c = 80$ wt%. One example consisting of five pairs of such legs is shown in Figure S2 (Supporting Information) and delivers a thermovoltage of 170 μV K^{-1} which is close to the sum of Seebeck coefficients of the constituting legs.

Since $c_p << c_s$, we argue that the majority of carriers for $c \approx 25$ wt% of CNTs are holes, or, in other words, holes are being transported through the CNTs, which is the electrically more conductive part of the composite. A possible explanation for this observation is that P3HT is effectively doping the CNTs.[41,42] This hypothesis is supported by photoluminescence (PL) quenching experiments (Figure 2d), which indicate that there is a strong photoinduced charge transfer between P3HT and CNTs.[43] The observed phenomenology regarding the thermoelectric properties of the nanocomposites can be well explained in terms of a simple band model,[44] which considers the semiconducting CNTs as being co-doped. The donor impurities correspond to the nitrogen atoms substitutionally incorporated during production of the CNTs, whereas the P3HT wrapped around the nanotubes is assumed to effectively act as an acceptor, injecting holes into the CNT valence band, as was very recently shown for CNT composites with polyelectrolytes.[45] The actual position of the Fermi level in the CNTs at a given temperature simply results from the difference in effective donor- and acceptor-level densities by invoking charge neutrality.[46] This determines the type of the majority carriers in the system, and in turn, the sign of the Seebeck coefficient as is explained in more detail in the discussion of Figure S3 (Supporting Information). This interpretation in terms of doping also explains why treatment of a 20 wt% P3HT/CNT composite with a p-dopant like $FeCl_3$ further increases the electrical conductivity ($FeCl_3$ dopes P3HT, which in turn dopes the CNTs), while the same dopant has no significant effect on an 80 wt% composite due to pinning of the Fermi level, as shown in Figure S4 (Supporting Information). Interestingly, samples

ADVANCED MATERIALS
www.advmat.de

www.MaterialsViews.com

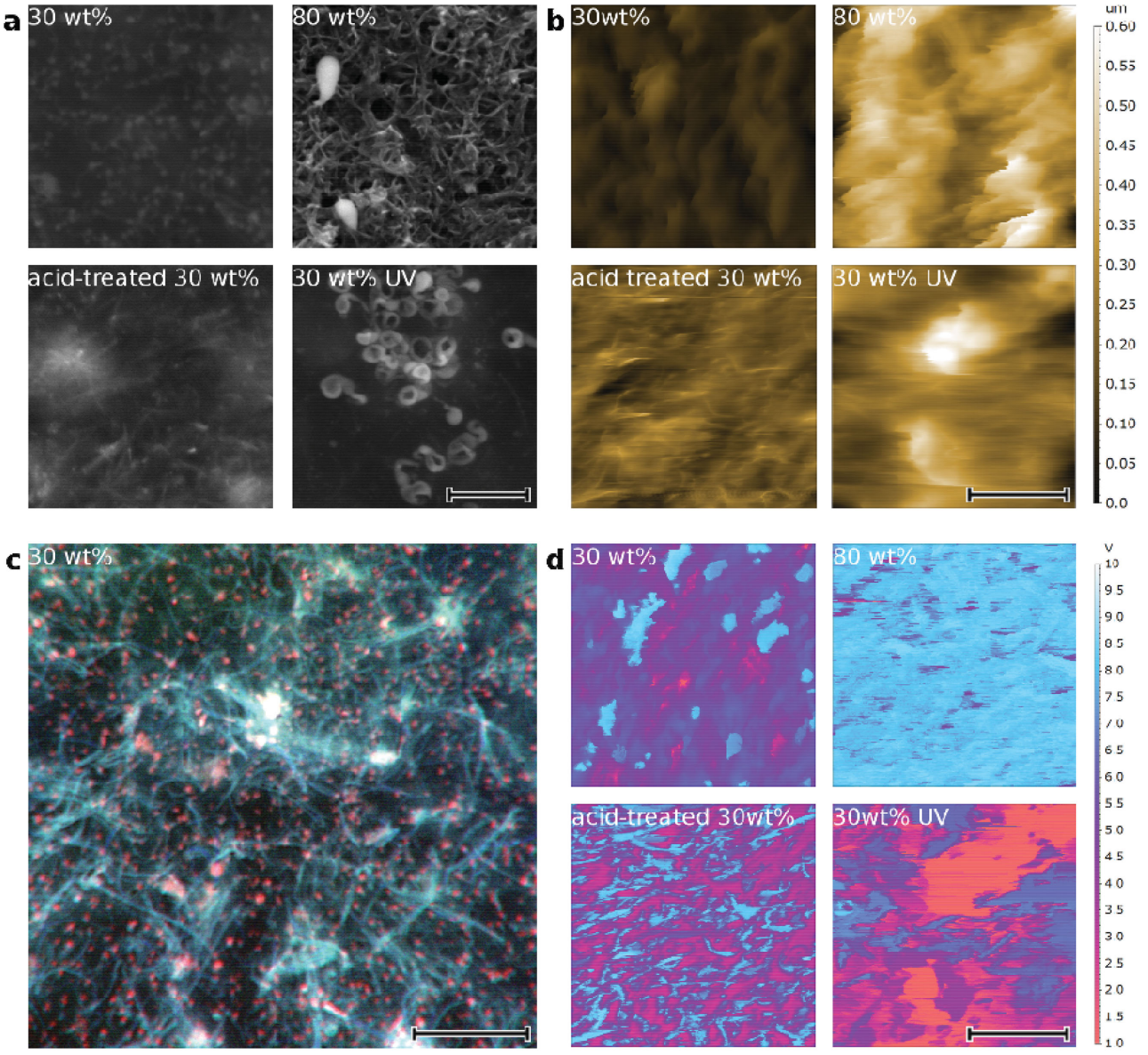

Figure 1. Nanostructure of four representative CNT-P3HT nanocomposites (from top left to bottom right: 30 wt% CNTs, 80 wt% CNTs, 30 wt% acid-treated CNTs, and 60s UV-treated 30 wt% CNTs). a) Scanning electron micrographs illustrating the sample surface. Varying amounts of CNT bundles and P3HT matrix are visible in all samples. Additionally, the 80 wt% samples contain Fe-catalyst, and in the UV-treated samples, scrap-like features are visible. b) AFM topography confirms that 80 wt% and UV-treated samples exhibit considerable roughness. c) False color transmission X-ray micrograph combining information on measurements at three distinct energies. Increased absorption due to nitrogen slightly above K_α(nitrogen) at 399 eV is pictured in blue. Increased absorption above L_α(iron) at 707 eV is represented in red. Variations due to sample thickness measured at 520 eV are represented in green. d) Conductive AFM measurements corresponding to the topography in (b). The color scale is proportional to the logarithm of the measured current. All scale bars are 2 μm.

based on acid-treated CNTs show a higher percolation threshold while retaining the n-character throughout the investigated composite fractions. We rationalize this behavior with a less effective p-doping of CNTs by P3HT due to a smaller interaction between components. This is supported by a less effective PL quenching (Figure 2d) and by having purer domains (cf. Figure S1, Supporting Information).

In composites biased close to the transition from p- to n-type by appropriately selecting the CNT content, small differences in doping are expected to produce large differences in Seebeck coefficient. To confirm this, we selected n-type samples of as-synthesized 40 wt% CNTs, and 5 wt% acid-treated CNTs. And indeed, the Seebeck coefficient can be changed to a positive value by doping the composites with $FeCl_3$ (data not shown).[24] The comparison between composites made from the two CNT batches suggests that the thermoelectric behavior of these composites strongly depends on the electronic properties of the matrix polymer as well as the specific interactions between P3HT and CNTs. So next we attempted to verify this hypothesis. Perhaps the simplest treatment is the application of

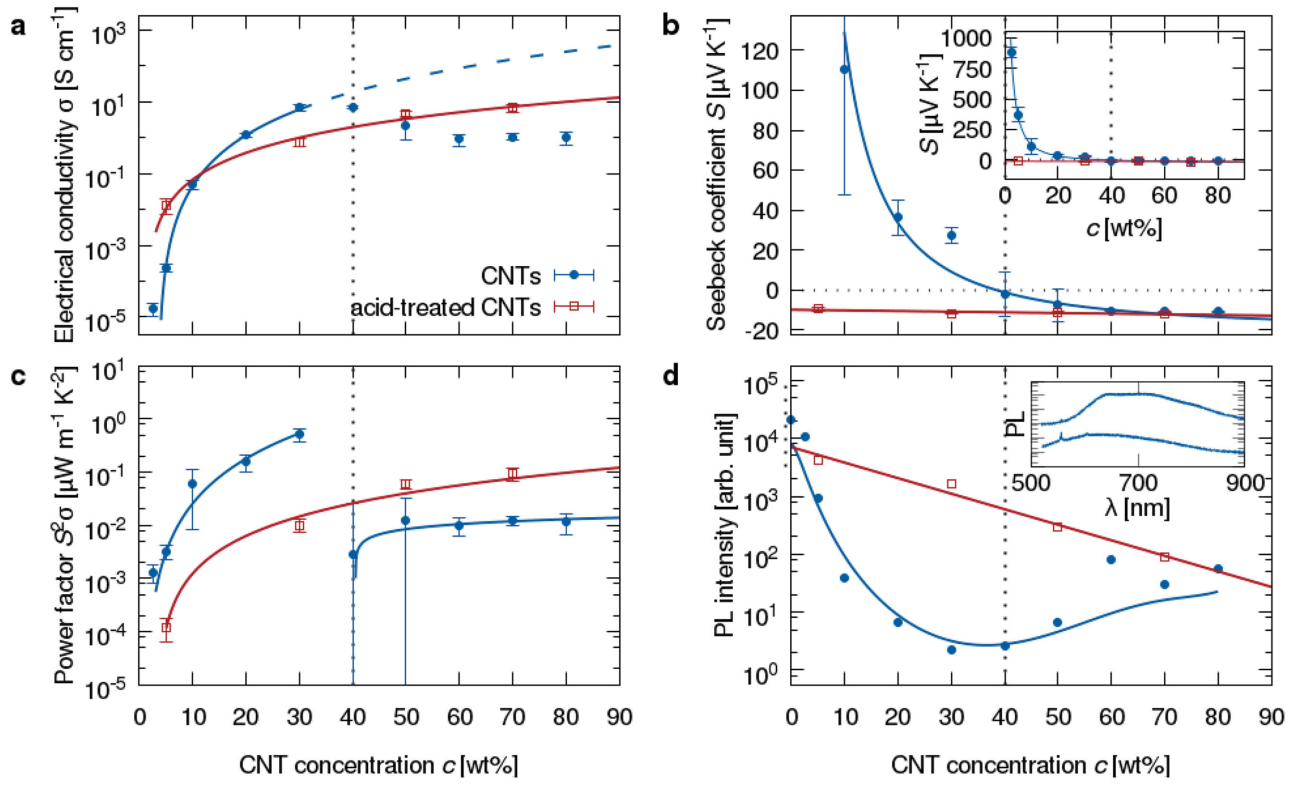

Figure 2. Dependence of thermoelectric properties on CNT concentration for as-synthesized (blue filled circles) and acid-treated CNTs (red open squares). a) σ shows percolative behavior, increasing by several orders of magnitude upon addition of a few wt% of CNTs. At high CNT content, a dip in σ is observed for as-synthesized CNTs. The dashed line sketches the expected behavior for similar composites prepared from regular, undoped CNTs. b) Correspondingly, S steadily decreases with increasing CNT concentration, and crosses over to negative values at $c_s = 40$ wt% CNTs. For higher CNT concentrations, S saturates at about –10 μV K^{-1}. For the acid-treated CNTs, S is independent of the CNT concentration in the investigated range. The inset shows the complete measured composition range. c) Resulting power factor $S^2\sigma$. For as-synthesized CNTs, two regions are apparent, one below c_s, where the composite has p-type properties, and another above c_s, where the material is n-type. d) Averaged PL intensity between 675 and 725 nm, for samples excited at 514 nm. The inset shows two representative spectra with $c = 0$ wt% and $c = 80$ wt%. Error bars indicate the standard deviation across two batches of six samples each.

heat to promote (partial) detachment of the P3HT chains from the CNT surface, thereby reducing polymer/CNT contact and concomitant doping. Indeed, these composites exhibit thermochromism in solution when heated. Upon increasing the temperature, the composite solution turns from a characteristic dark purple, indicative of π-stacked, crystalline P3HT, to the bright orange coloration associated with well dissolved, isolated P3HT. Unfortunately, this change is not preserved through the transition to the dried film, as no changes of the thermoelectric properties are observed. Conversely, a reference P3HT solution does not show any thermochromism during preparation and subsequent heating.

Another conceivable treatment that is easily implemented is the irradiation of the solution by UV-light. Excitingly, this treatment does confirm our hypothesis above. For samples that were UV-irradiated while drying using a low pressure mercury vapor lamp, the Seebeck coefficient continuously decreases as a function of irradiation time for the investigated samples, which contain 20 and 30 wt% CNTs (**Figure 3**a). For the 30 wt% samples, S becomes negative after 60 s of UV-irradiation. These results open the possibility to creating thermoelectric generators with p- and n-legs from a single solution, as we will show below.

In order to understand the impact of UV-irradiation on the thermoelectric properties, we next investigate its effect on the structural and optical properties of the composites. Optical microscopy indicates that long exposure times (≥120 s) yield visibly degraded samples (Figure S5, Supporting Information). AFM also suggests an increase in surface roughness (Figure 1b), while SEM evidences the appearance of small curled scraps (Figure 1a), that are electrically insulating (Figure 1d and Figure S2, Supporting Information), which we ascribe to degraded polymer. Raman scattering suggests that UV-light has no negative effect on the CNTs (as measured by the ratio of the D- and G-bands, Figure S6, Supporting Information). Overall, long exposure times clearly degrade the samples and as a result, the macroscopic electrical conductivity also slightly decreases (Figure S7, Supporting Information).

Figure 3b shows the normalized absorption and PL intensities of four samples irradiated for 0, 60, 150, and 240 s. The aforementioned degradation is here seen as an absorption blueshift, due to a reduction in conjugation length of the polymer. The PL quenching that we discussed before is, upon UV irradiation, much less pronounced, demonstrating a lower degree of charge transfer between degraded polymer chains and CNTs, with the concomitant smaller degree of p-doping of

ADVANCED MATERIALS
www.advmat.de

www.MaterialsViews.com

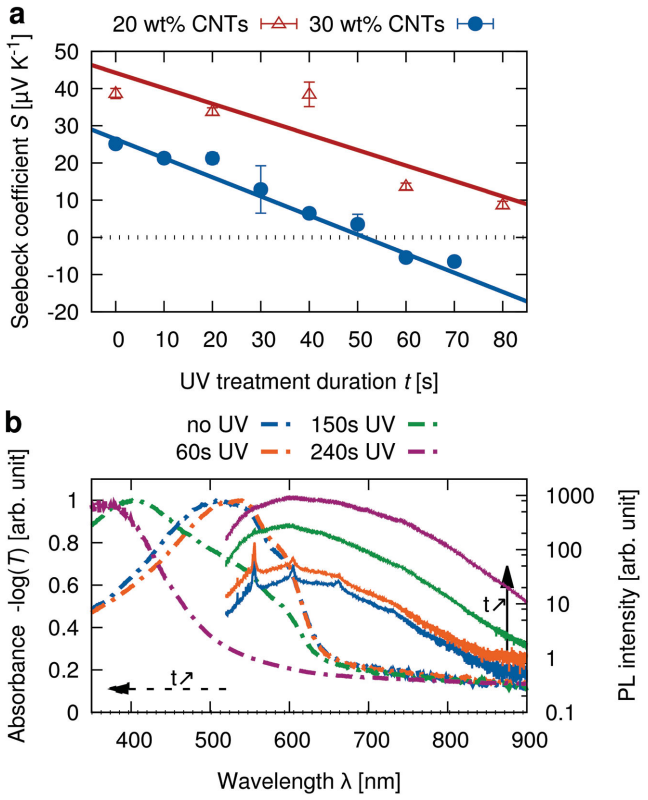

Figure 3. Sample properties after UV-irradiation during deposition. a) Seebeck coefficient versus UV treatment duration t for samples containing 20 wt% CNTs (red open triangles) and 30 wt% CNTs (blue filled circles). The lines serve as a guide to the eye. The error bars represent the standard deviation. b) Normalized absorbance (dashed lines) and PL spectra (solid lines) of 20 wt% CNT samples that have been irradiated for different amounts of time.

the CNTs. Photodegradation of P3HT in thin films has indeed been well studied.[47,48] Photobleaching has been observed with an additional blueshift of the absorption associated to an ozone mediated decrease of the average length of π-conjugation.[49] In solution, on the other hand, the blueshift is not necessarily caused by ozone, but simple UV irradiation in an oxygen containing atmosphere is already sufficient.[50] Both photobleaching in the presence of singlet oxygen, and chain scission have been observed, where the chain scission is induced by the presence of $FeCl_3$ residue in the sample.[51]

Figure 3b also shows that there are two clear regimes: For short exposure times (<60 s), there is little degradation of the polymer (no photobleaching, no absorption blueshift, high degree of PL quenching) but a strong change in the electronic properties, as observed by the change in Seebeck sign. Long exposure times (>120 s) result in complete degradation of the polymer with destructive effects on the electronic properties. This kind of induction period during which properties at first only change slowly, is a common observation during UV-degradation of polymers.[52] The Fourier transform infrared (FTIR) spectra shown in Figure S8 (Supporting Information) back up this observation, and provide evidence that the UV treatment attacks both the carbon double bonds of the thiophene ring, as well as the alkyl side chains, influencing the doping not only by reducing conjugation, but also by impairing the CNT–P3HT interaction.

There is, therefore, a reasonable processing window to modify the thermoelectric properties of the composites by UV irradiation before unwanted degradation occurs. In order to illustrate the potential advantages of such a method, we have realized a thermoelectric module fabricated from a single solution with p- and (UV-irradiated) n- legs. **Figure 4** illustrates a proof of concept thermoelectric module and some envisaged applications that are implemented through a toroidal geometry of the module. First a uniform wet layer of the composite is deposited, and half of it is UV-irradiated during drying (Figure 4a). In a second step, the individual legs are patterned by appropriate cutting (Figure 4b). We connected p- and n-type legs with silver paste in order to strengthen the bridge region. (Note that these contacts are not strictly needed, since they provide no increase in conductance for an in-plane current in a layer of homogeneous thickness.) In a third step, the device is folded into a spiral, and adjacent couples are connected electrically in series by depositing contacts (Figure 4c). In the last step, the ends of this spiral are joined to form a torus (Figure 4d,e). Figure 4g shows one conceivable application as a wristband. When one side of this module comprising 15 double legs is attached to a glass filled with ice water, leaving the other side at room temperature, it generates a voltage of 5 mV which corresponds to 217.4 μV K^{-1} in total or 14.5 μV K^{-1} per couple. A plot of the output current and power versus voltage is given in Figure S9 (Supporting Information). The module supplies ≈2 nA at 5 mV Seebeck voltage. An alternative geometry may allow connecting a larger number of legs to harvest, for instance, waste heat from a pipe. For this, the spiral itself can be wound into yet another spiral, as in Figure 4f.

Importantly, we have measured the bulk thermal conductivity of selected 1 mm thick samples and verify that κ only slightly increases from 0.29 W m^{-1} K^{-1} for neat P3HT to 0.55 W m^{-1} K^{-1} for a c = 80 wt% composite (see **Table 1** and Table S1, Supporting Information). The nonoptimized ZT values are then around 10^{-3} and 10^{-5} for the p-type and n-type composite, respectively. Despite being relatively low, these values are similar to recently reported n-type organic materials which exhibited power factors around 0.1–1 μW m^{-1} K^{-2} (cf. 0.01 μW m^{-1} K^{-2} for this work).[5,6] Since the presented method is likely to be applicable to other materials systems, we expect that significantly higher efficiencies can be reached by selecting better performing materials like semiconducting single-walled carbon nanotubes, and appropriate dopants,[53] while keeping processing complexity low by depositing a minimum number of layers and selecting a suitable transformation step like the UV-irradiation presented here, or other simple methods, like vapor printing.[54]

Besides performance, stability is also a key parameter since most reported n-type organic materials are not stable in air. In our case, all samples were prepared, measured and stored in atmosphere. Figure S10 (Supporting Information) shows the results of repeated electrical measurements carried out over a period of up to 600 d. The negative Seebeck coefficient was stable for all measured n-type samples, with no significant changes observed after 240 d for any of the high CNT content and UV-treated samples. In the same amount of time, the

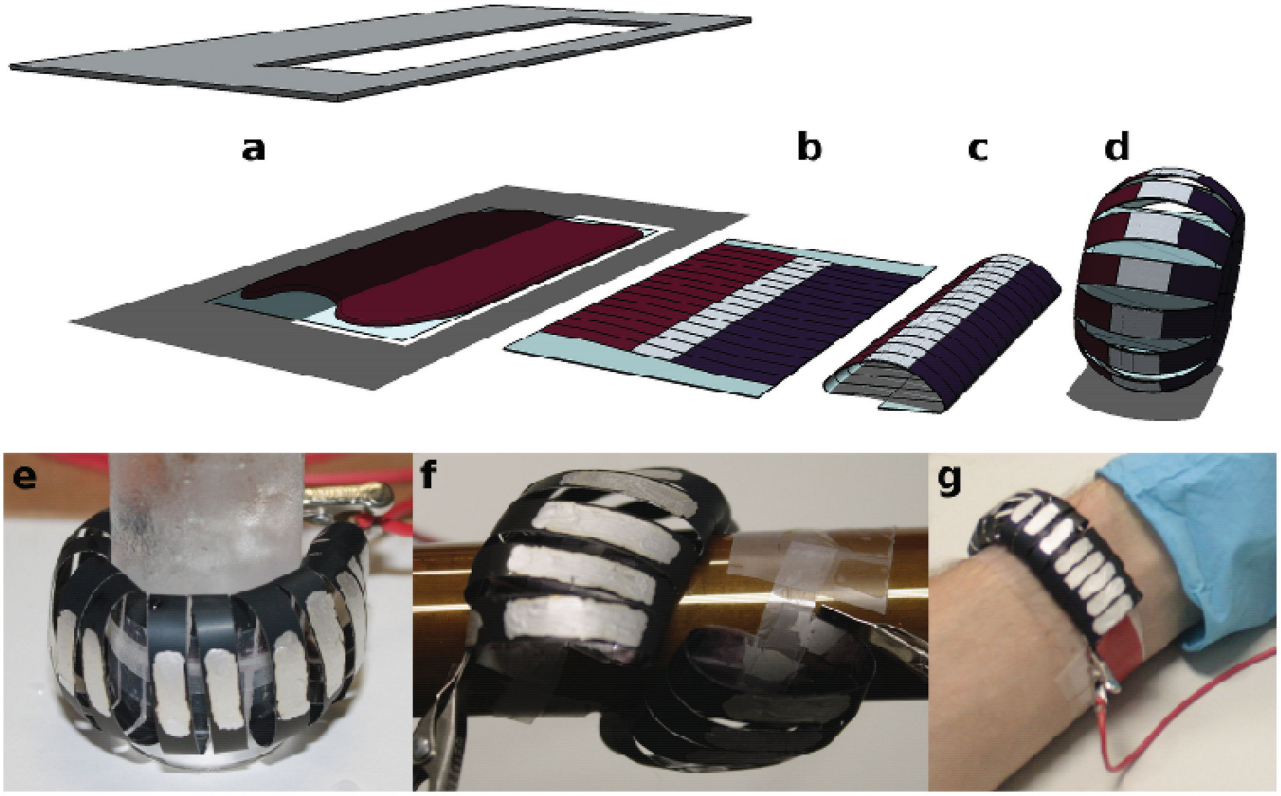

Figure 4. Proposed fabrication and applications of a device geometry that plays on the advantages of the presented material. a) A large area is coated from a single solution, and patterned by UV irradiation. b) If desired, additional contacts (on what will be the outer side) are deposited. c) The flexibility of the PET substrate is employed to easily connect the couples electrically in series by depositing contacts at what will be the inner side of the torus. d) The final toroidal device geometry. Possible application geometries in the form of e) a single torus, f) an extended spiral, and g) a wristband. The width of a single leg of the pictured device is 5 mm.

electrical conductivity did not decrease by more than half of the initial value and then remained stable for subsequent measurements after 600 d.

In summary, we have shown that P3HT-CNT composites can exhibit either a positive or negative Seebeck coefficient depending on stoichiometry. Furthermore we have demonstrated photoinduced switching of p-type to n-type composites, which simplifies the fabrication of thermoelectric modules by requiring only a single solution. This way, processing complexity can be reduced by using large area coating instead of more complex additive printing processes. Finally we have fabricated proof-of-principle wearable thermoelectric modules using the developed methods.

Table 1. Bulk thermal conductivity κ of 1 mm thick P3HT/CNT samples. For a summary of the complete measured data, including density ρ, specific heat capacity C_p, and thermal diffusivity α, see Table S1 (Supporting Information).

	Thermal conductivity κ [W m^{-1} K^{-1}]
Neat P3HT	0.29 ± 0.01
30 wt% CNTs	0.40 ± 0.03
30 wt% acid-treated CNTs	0.49 ± 0.02
80 wt% CNTs	0.55 ± 0.04

Experimental Section

Materials: Nitrogen doped multiwalled carbon nanotubes were synthesized from a saturated solution of acetonitrile/ferrocene feedstock by a chemical vapor deposition using a continuous process.[39,40,55–57] CNTs contain approximately 7 wt% nitrogen, as determined by scanning transmission electron microscopy/electron energy loss spectroscopy. The CNTs typically contained residual iron from the catalyst used in their formation. In order to minimize available iron, a sample of the nanotubes was heated at reflux first in concentrated aqueous HCl for 18 h, followed by extensive washing with water, and then heated in refluxing acetic acid for 24 h, again followed by extensive washing with water. Poly(3-hexylthiophene-2,5-diyl) (P3HT, $M_w \approx 97$ kg mol^{-1}, $M_w/M_n \approx 2.4$, regioregularity >90%, Rieke Metals), oDCB (99% ReagentPlus) and chloroform (>99.9% CHROMASOLV) were obtained from Sigma-Aldrich. All materials were used as received.

Solution Preparation: CNTs were dispersed in oDCB at a concentration of 1 g L^{-1} and sonicated in ice water for 60 min (JP Selecta Ultrasons 50W). P3HT was dissolved in chloroform at a concentration of 20 g L^{-1} and an appropriate amount was added in three steps to the CNT dispersion to create a mixture with the desired CNT concentration. After each addition, the mixture was sonicated an additional 30 min in ice water. After a day, a precipitate of residual carbon and sedimented CNTs can be observed, the remaining solution was stable for months.

Sample Preparation: 1.5 mL of solution was drop-cast onto PET substrates and left to evaporate. Some samples were irradiated with 50 mW cm^{-2} of UV-light directly after deposition in a Jelight UVO-Cleaner 42.

Electrical Characterization: The Seebeck coefficient was measured at 300 K and ambient atmosphere with an SB1000 instrument equipped with

a K2000 temperature controller from MMR Technologies using a thermal load of about 1–2 K and a constantan wire as an internal reference. For each composition, six 5 × 1 mm^2 small samples from two independently prepared films were measured; each measurement was repeated ten times. Samples were contacted with silver paste from Agar Scientific.

The electrical conductivity measurements were performed on separate samples from the same batch. Four silver paste contacts were placed in the corners of the 1 cm × 1 cm samples. Conductivity was measured with an Ecopia HMS-5000 Hall measurement system, using the van der Pauw method.[58]

Bulk Thermal Conductivity: Samples for thermal conductivity measurements were prepared by (1) solidifying material from combined 1 g L^{-1} CNTs in oDCB and 20 g L^{-1} P3HT in $CHCl_3$ solutions, (2) compacting material at ambient temperature and a pressure of 18.5 kN cm^{-2} to form two identical round pellets with a diameter of 13 mm and thickness of 1 mm, and (3) hot-pressing pellets at 150 °C at a pressure of less than 7.4 kN cm^{-2}. The density was estimated by measuring the volume and weight of the pellets. The heat capacity and thermal diffusivity were measured at ambient temperature with a TPS 2500 S Thermal Constants Analyser from Hot Disk AB using an isotropic model.

Physical Characterization: Sample thickness was measured using a KLA Tencor MicroXAM-100 optical surface profilometer for samples with 50 wt% CNTs and below. Samples with higher CNT concentration were measured using a KLA Tencor P16+ profilometer. The sample thickness ranged between 15 and 0.8 µm, depending on the total solution concentration. For high CNT wt% composites, the samples contained a significant amount of voids, and consequently the total amount of material is overestimated and σ underestimated accordingly.

Optical Characterization: Transmission spectra of samples were measured using a GES-5E ellipsometer from Sopralab. Raman and photoluminescence spectra were measured in backscattering configuration with a LabRam HR800 spectrometer (Horiba Jobin Yvon) coupled with a confocal Olympus microscope, using 514 and 633 nm excitation wavelengths. Raman imaging was performed using a Witec alpha300 R confocal equipment (532 nm excitation). FTIR spectra were measured using a Perkin–Elmer Spectrum One spectrometer coupled to a universal attenuated total reflectance accessory.

Optical micrographs were taken using an Olympus BX51 optical microscope and a DP20 microscope digital camera.

Structural Characterization: Scanning electron microscopy was conducted using a FEI Quanta 200 FEG. AFM and current sensing AFM were measured using an Agilent 5500LS instrument with a Rocky Mountain Nanotechnology solid platinum tip. TXM was conducted at the MISTRAL beamline at the ALBA synchrotron.[59,60] For this, samples were drop-cast onto copper grids.

Supporting Information

Supporting Information is available from the Wiley Online Library or from the author.

Acknowledgements

The authors would like to thank Dr. Isabel Alonso (ICMAB) and Prof. Salvador Ferrer (ALBA) for assisting during the synchrotron sessions as well as for useful discussions. The authors would also like to acknowledge financial support from the Ministerio de Economía y Competitividad of Spain through projects CSD2010–00044 (Consolider NANOTHERM) and MAT2012–37776 and the European Research Council (ERC) under grant agreement nos. 637624 and 648901. C.M. gratefully acknowledges financial support from Formas, the Knut and Alice Wallenberg Foundation through a Wallenberg Academy Fellowship. The transmission X-ray microscopy experiments were performed at MISTRAL beamline at ALBA Synchrotron with the collaboration of ALBA staff. A.E.B. thanks the Egyptian Ministry of Higher Education for funding through the Short-term Scientific Mission Postdoctoral program. The authors thank Dr. Elena Bailo (Witec) for assistance with the Raman imaging experiments.

Received: November 9, 2015
Revised: December 9, 2015
Published online: February 8, 2016

[1] Y. Liu, J. Zhao, Z. Li, C. Mu, W. Ma, H. Hu, K. Jiang, H. Lin, H. Ade, H. Yan, *Nat. Commun.* **2014**, *5*, 5293.
[2] C.-C. Chen, W.-H. Chang, K. Yoshimura, K. Ohya, J. You, J. Gao, Z. Hong, Y. Yang, *Adv. Mater.* **2014**, *26*, 5670.
[3] C. Cho, B. Stevens, J.-H. Hsu, R. Bureau, D. A. Hagen, O. Regev, C. Yu, J. C. Grunlan, *Adv. Mater.* **2015**, *27*, 2996.
[4] G. Kim, L. Shao, K. Zhang, K. P. Pipe, *Nat. Mater.* **2013**, *12*, 719.
[5] B. Russ, M. J. Robb, F. G. Brunetti, P. L. Miller, E. E. Perry, S. N. Patel, V. Ho, W. B. Chang, J. J. Urban, M. L. Chabinyc, C. J. Hawker, R. A. Segalman, *Adv. Mater.* **2014**, *26*, 3473.
[6] R. A. Schlitz, F. G. Brunetti, A. M. Glaudell, P. L. Miller, M. A. Brady, C. J. Takacs, C. J. Hawker, M. L. Chabinyc, *Adv. Mater.* **2014**, *26*, 2825.
[7] T. R. Andersen, H. F. Dam, M. Hösel, M. Helgesen, J. E. Carlé, T. T. Larsen-Olsen, S. A. Gevorgyan, J. W. Andreasen, J. Adams, N. Li, F. Machui, G. D. Spyropoulos, T. Ameri, N. Lemaître, M. Legros, A. Scheel, D. Gaiser, K. Kreul, S. Berny, O. R. Lozman, S. Nordman, M. Välimäki, M. Vilkman, R. R. Søndergaard, M. Jørgensen, C. J. Brabec, F. C. Krebs, *Energy Environ. Sci.* **2014**, *7*, 2925.
[8] R. R. Søndergaard, M. Hösel, N. Espinosa, M. Jørgensen, F. C. Krebs, *Energy Sci. Eng.* **2013**, *1*, 81.
[9] A. Pierre, M. Sadeghi, M. M. Payne, A. Facchetti, J. E. Anthony, A. C. Arias, *Adv. Mater.* **2014**, *26*, 5722.
[10] H. Sirringhaus, *Science* **1998**, *280*, 1741.
[11] O. Bubnova, Z. U. Khan, A. Malti, S. Braun, M. Fahlman, M. Berggren, X. Crispin, *Nat. Mater.* **2011**, *10*, 429.
[12] M. F. Ashby, *Acta Metall.* **1989**, *37*, 1273.
[13] *Polymer Handbook* (Eds: J. Brandrup, E. H. Immergut, E. A. Grulke), John Wiley & Sons, New York **2003**.
[14] S. Shen, A. Henry, J. Tong, R. Zheng, G. Chen, *Nat. Nanotechnol.* **2010**, *5*, 251.
[15] M. M. Rojo, J. Martín, S. Grauby, T. Borca-Tasciuc, S. Dilhaire, M. Martin-Gonzalez, *Nanoscale* **2014**, *6*, 7858.
[16] D. Hansen, G. A. Bernier, *Polym. Eng. Sci.* **1972**, *12*, 204.
[17] A. J. Heeger, *Rev. Mod. Phys.* **2001**, *73*, 681.
[18] K. C. See, J. P. Feser, C. E. Chen, A. Majumdar, J. J. Urban, R. A. Segalman, *Nano Lett.* **2010**, *10*, 4664.
[19] C. Yu, K. Choi, L. Yin, J. C. Grunlan, *ACS Nano* **2011**, *5*, 7885.
[20] O. Bubnova, Z. U. Khan, H. Wang, S. Braun, D. R. Evans, M. Fabretto, P. Hojati-Talemi, D. Dagnelund, J.-B. Arlin, Y. H. Geerts, S. Desbief, D. W. Breiby, J. W. Andreasen, R. Lazzaroni, W. M. Chen, I. Zozoulenko, M. Fahlman, P. J. Murphy, M. Berggren, X. Crispin, *Nat. Mater.* **2014**, *13*, 190.
[21] M. Culebras, C. M. Gómez, A. Cantarero, *J. Mater. Chem. A* **2014**, *2*, 10109.
[22] K. Suemori, Y. Watanabe, S. Hoshino, *Appl. Phys. Lett.* **2015**, *106*, 113902.
[23] B. Abad, I. Alda, P. Díaz-Chao, H. Kawakami, A. Almarza, D. Amantia, D. Gutierrez, L. Aubouy, M. Martín-González, *J. Mater. Chem. A* **2013**, *1*, 10450.
[24] C. Bounioux, P. Díaz-Chao, M. Campoy-Quiles, M. S. Martín-González, A. R. Goñi, R. Yerushalmi-Rozen, C. Müller, *Energy Environ. Sci.* **2013**, *6*, 918.
[25] S. L. Kim, K. Choi, A. Tazebay, C. Yu, *ACS Nano* **2014**, *8*, 2377.

[26] C. A. Hewitt, A. B. Kaiser, S. Roth, M. Craps, R. Czerw, D. L. Carroll, *Appl. Phys. Lett.* **2011**, *98*, 183110.
[27] C. A. Hewitt, A. B. Kaiser, S. Roth, M. Craps, R. Czerw, D. L. Carroll, *Nano Lett.* **2012**, *12*, 1307.
[28] C. A. Hewitt, D. S. Montgomery, R. L. Barbalace, R. D. Carlson, D. L. Carroll, *J. Appl. Phys.* **2014**, *115*, 184502.
[29] T. Fukumaru, T. Fujigaya, N. Nakashima, *Sci. Rep.* **2015**, *5*, 7951.
[30] K. Yanagi, S. Kanda, Y. Oshima, Y. Kitamura, H. Kawai, T. Yamamoto, T. Takenobu, Y. Nakai, Y. Maniwa, *Nano Lett.* **2014**, *14*, 6437.
[31] Y. Nonoguchi, K. Ohashi, R. Kanazawa, K. Ashiba, K. Hata, T. Nakagawa, C. Adachi, T. Tanase, T. Kawai, *Sci. Rep.* **2013**, *3*, 3344.
[32] A. M. Marconnet, N. Yamamoto, M. A. Panzer, B. L. Wardle, K. E. Goodson, *ACS Nano* **2011**, *5*, 4818.
[33] A. Nish, J.-Y. Hwang, J. Doig, R. J. Nicholas, *Nat. Nanotechnol.* **2007**, *2*, 640.
[34] F. Jakubka, S. P. Schießl, S. Martin, J. M. Englert, F. Hauke, A. Hirsch, J. Zaumseil, *ACS Macro Lett.* **2012**, *1*, 815.
[35] S. K. Samanta, M. Fritsch, U. Scherf, W. Gomulya, S. Z. Bisri, M. A. Loi, *Acc. Chem. Res.* **2014**, *47*, 2446.
[36] H. W. Lee, Y. Yoon, S. Park, J. H. Oh, S. Hong, L. S. Liyanage, H. Wang, S. Morishita, N. Patil, Y. J. Park, J. J. Park, A. Spakowitz, G. Galli, F. Gygi, P. H. Wong, J. B. Tok, J. M. Kim, Z. Bao, *Nat. Commun.* **2011**, *2*, 541.
[37] W. Gomulya, G. D. Costanzo, E. J. F. de Carvalho, S. Z. Bisri, V. Derenskyi, M. Fritsch, N. Fröhlich, S. Allard, P. Gordiichuk, A. Herrmann, S. J. Marrink, M. C. Dos Santos, U. Scherf, M. A. Loi, *Adv. Mater.* **2013**, *25*, 2948.
[38] A. Kumar, M. A. Baklar, K. Scott, T. Kreouzis, N. Stingelin-Stutzmann, *Adv. Mater.* **2009**, *21*, 4447.
[39] D. Qian, R. Andrews, M. S. Meier, M. Weisenberger, M. S. Meier, *Nanomater. Energy* **2012**, *1*, 168.
[40] D. Qian, R. Andrews, D. Jacques, P. Kichambare, G. Lian, E. C. Dickey, *J. Nanosci. Nanotechnol.* **2003**, *3*, 93.
[41] N. M. Dissanayake, Z. Zhong, *Nano Lett.* **2011**, *11*, 286.
[42] M. Shim, A. Javey, N. W. Shi Kam, H. Dai, *J. Am. Chem. Soc.* **2001**, *123*, 11512.
[43] S. D. Stranks, C. Weisspfennig, P. Parkinson, M. B. Johnston, L. M. Herz, R. J. Nicholas, *Nano Lett.* **2011**, *11*, 66.
[44] L. Bergmann, C. Schaefer, *Lehrbuch Der Experimentalphysik - Band 6: Festkörper*, Walter De Gruyter, Berlin **1992**.
[45] C.-K. Mai, B. Russ, S. L. Fronk, N. Hu, M. B. Chan-Park, J. J. Urban, R. A. Segalman, M. L. Chabinyc, G. C. Bazan, *Energy Environ. Sci.* **2015**, *8*, 2341.
[46] M. He, J. Ge, Z. Lin, X. Feng, X. Wang, H. Lu, Y. Yang, F. Qiu, *Energy Environ. Sci.* **2012**, *5*, 8351.
[47] M. Manceau, A. Rivaton, J.-L. Gardette, S. Guillerez, N. Lemaître, *Polym. Degrad. Stab.* **2009**, *94*, 898.
[48] H. Hintz, H.-J. Egelhaaf, L. Lüer, J. Hauch, H. Peisert, T. Chassé, *Chem. Mater.* **2011**, *23*, 145.
[49] H. Hintz, H.-J. Egelhaaf, H. Peisert, T. Chassé, *Polym. Degrad. Stab.* **2010**, *95*, 818.
[50] S. Holdcroft, *Macromolecules* **1991**, *24*, 4834.
[51] M. S. A. Abdou, S. Holdcroft, *Macromolecules* **1993**, *26*, 2954.
[52] *Ultraviolet Light Induced Reactions in Polymers* (Ed: S. S. Labana), American Chemical Society, Washington, D. C. **1976**.
[53] H. Wang, J.-H. Hsu, S.-I. Yi, S. L. Kim, K. Choi, G. Yang, C. Yu, *Adv. Mater.* **2015**, *27*, 6855.
[54] D. Nassyrov, C. Müller, A. Roigé, I. Burgués-Ceballos, J. Oriol Ossó, D. B. Amabilino, M. Garriga, M. Isabel Alonso, A. R. Goñi, M. Campoy-Quiles, *J. Mater. Chem.* **2012**, *22*, 4519.
[55] I. Kunadian, R. Andrews, M. P. Mengüç, D. Qian, *Carbon* **2009**, *47*, 589.
[56] D. N. Jacques, R. J. Andrews (University of Kentucky Research Foundation), *US7160531*, **2007**.
[57] D. N. Jacques, R. J. Andrews (University of Kentucky Research Foundation), *US7504078*, **2009**.
[58] L. J. van der Pauw, *Philips Tech. Rev.* **1958**, *20*, 220.
[59] E. Pereiro, J. Nicolás, S. Ferrer, M. R. Howells, *J. Synchrotron Radiat.* **2009**, *16*, 505.
[60] A. Sorrentino, J. Nicolás, R. Valcárcel, F. J. Chichón, M. Rosanes, J. Avila, A. Tkachuk, J. Irwin, S. Ferrer, E. Pereiro, *J. Synchrotron Radiat.* **2015**, *22*, 1112.